Experimental investigation of oxidation resistance of SiC powder for the protection of re-entry space vehicle using material shock tube

Jayaram Vishakantaiah[1*], Gowtham Balasubramaniam[2]

[1]*Shock Induced Materials Chemistry Laboratory, SSCU, Indian Institute of Science, Bengaluru 560012, India*
[2]*Laboratory For Hypersonic and Shock Wave Research, Department of Aerospace Engineering,
Indian Institute of Science, Bengaluru 560012, India*

*Corressponding author

Abstract

A novel method of studying oxidation resistance and phase transformation of SiC fine powder was performed using multiple shock treatments in millisecond timescale using indigenously developed material shock tube (MST1). MST1 was used to produce shock waves which heat the ultra high pure oxygen test gas to a reflected shock temperature and pressure of about 5300 K (estimated) and 25 bar, respectively for 1-2 milliseconds. Different characterization techniques like X-ray diffraction (XRD), scanning electron microscopy (SEM), transmission electron microscopy (TEM) and X-ray photoelectron spectroscopy (XPS) show the formation of oxides and sub-oxide species after shock treatment. XRD studies shows the phase transformation of hexagonal SiC to amorphous SiO_2. SEM and TEM micrographs show change in surface morphology of SiC from irregular shape to micro/nano spheres due to superheating and cooling at the rate of about 10^6 K/s. This novel method is used for the first time to demonstrate the behavior of material in presence of extreme aero-thermodynamic conditions for a short duration. These conditions generated using shock tubes are not achievable by conventional furnaces for oxidation studies of SiC in a short duration. Copyright © 2018 VBRI Press.

Keywords: Dynamic shock treatment, oxidation of SiC, gas-solid interaction, high temperature ceramic, non-catalytic reactions.

Introduction

Thermal protection systems (TPS) materials are used in advanced hypersonic vehicles to withstand in the high temperature during atmospheric entry. The demand for advanced TPS related to re-entry vehicles has led the development of different classes of ultra-high temperature ceramic (UHTC) composites for use in extreme aero-thermodynamic conditions, where temperatures reach above 2000°C. There are varieties of UHTC materials made out of compounds such as SiO_2, $MoSi_2$, HfB_2, TiC, ZrB_2 etc. and their composites. To improve the oxidation resistance property of TPS materials SiC is used as an additive. SiC-based composites have been widely studied for applications in hot structures of space vehicles and missiles [1−4]. SiC have significant properties like high melting point, high thermal and chemical stability, low temperature coefficient of expansion, etc. [5]. Si-SiC cellular ceramics are used in applications such as porous burners, heat exchangers, structural ceramic sandwiches, concentrated solar radiation absorbers, electric heaters etc. [6]. SiC and Si based materials are also used in micro electro mechanical systems (MEMS) sensors for aerospace applications [7]. SiC undergoes both active and passive oxidation in presence of oxygen atmosphere [8]. Many studies have been undertaken to investigate oxidation of SiC, resulting in the formation metastable phase of sub-oxycarbides like $SiOC_3$, SiO_2C_2, SiO_3C and sub oxides such as SiO_2, SiO and Si_2O_3 [8, 9]. Studies with composites such as ZrB_2 with SiC at various percentages exhibited excellent oxidation resistance even at higher temperatures of about 2000°C [10, 11]. Researchers have also carried out works to measure the tensile strength, fracture behavior, porosity of C/SiC composite and SiC [12−14]. Oxidation resistance experiments done above 1700°C on HfB_2-SiC monolithic coatings have revealed that a borosilicate glass layer is formed at low temperatures which helps for further oxidation resistance upto 1000°C [15]. SiC nanofibers are used along with SiO_2 thin films to improve oxidation resistance of graphite substrate [16]. SiC has become an important component in most of the UHTC materials to increase the oxidation resistance properties due to its reaction towards oxygen. It also has capability to react with nitrogen at higher temperatures and the resulting species containing Si_3N_4 and other related nitrogen mixed species [17]. Previously researchers have used light gas gun to accelerate a flyer to velocities of about 1.5 ~ 4.6 km/s

to produce a high pressure to interact with SiC and other kind of tests are also done using thermal shocks [18−21]. Thin films of SiC have also been studied using free piston driven shock tube (FPST) with shock heated O_2 test gas at a reflected shock pressure P_5 of 60−70 bar and temperature T_5 (estimated) of about 8000 K to study its oxidation properties [22]. Apart from other characteristics, silicon related materials such as SiC, SiO_2 and Si_3N_4 exhibit good emissivity [23]. If oxygen partial pressure is high , it actively involves in oxidation and ablates, but lower oxygen partial pressures contributes to passive oxidation and formation of protective SiO_2 layer on SiC surface. Even after the formation of SiO_2 it maintains good emissivity which indirectly helps to protect the re-entry vehicle and other applications in hot structures. So it is important to study oxidation resistance and phase transformation of SiC under extreme thermodynamic conditions.

A novel experimental method of treating SiC fine powder to strong gas shock environment is presented in this work which is quite different from the conventional shock produced by flyer/projectile impact. This experimental method replicates the aero-thermodynamic conditions to simulate the reaction mechanism of SiC-based TPS materials during atmospheric re-entry conditions. Material shock tube (MST1) has been used to heat Ar + O_2 gas mixture to a very high temperature and at medium reflected shock pressure for a short duration. Similar kind of shock exposure study on ceramics like ZrO_2 were carried out using a high enthalpy shock tube facility called free piston driven shock tube (FPST) [24]. Due to the thermodynamic condition generated by MST1, O_2 goes to non-equilibrium state with vibrational, rotational excitation and dissociation state. This paper explores the possible phase transformation, oxidation and formation of various species due to the oxidation of SiC using shock treatment. After each successful shock treatment, the powder samples have been characterized using various experimental techniques.

Experimental

Experiments were performed on pristine SiC fine powders with a hexagonal crystal structure having JCPDS No. 01-074-1302 (procured from Alfa Aesar) using shock waves generated in MST1 facility operating at a stagnation enthalpy of about 4 MJ/kg. MST1 consists of a driver and driven section of 2 and 5 m long with an inner diameter of 80 mm. The high pressure driver section is separated from a low pressure driven section by the aluminium diaphragm. The driven section was purged with ultra-high pure (UHP) argon gas and evacuated to high vacuum up to 5×10^{-5} mbar. After attaining high vacuum the shock tube was filled with UHP (99.999%) argon and oxygen mixture with equal partial pressure of 0.025 bar. High pressure helium gas was filled into the driver section which ruptured the diaphragm. An arrangement to mount SiC fine powder was made on one side of the 0.4 m long

SiC reaction chamber as shown in the **Fig. 1**. SiC fine powder of required quantity (0.15 g) was mounted in the sample mounting flange, which interacted with the shock heated O_2 test gas. The pressure transducers (PCB Piezotronics Model No. 113B22) are mounted at various locations to acquire pressure signals and are recorded by a Tektronix digital oscilloscope (Model no. TBS2014B). The primary shock wave (at pressure P_2) travels inside the driven section and produces reflected shock wave (at pressure P_5) as it gets reflected at the end flange of the driven section. The time taken by the shock wave (Δt) to cross the two given sensor location at known distance (Δx) is used to find out the shock speed (V_S). The shock Mach number (M_S) thus calculated is used to calculate the reflected shock temperature (T_5) using 1-D normal shock relations shown in the following equations [25]:

$$V_S = \frac{\Delta x}{\Delta t} ; M_S = \frac{V_S}{a} = \frac{V_S}{\sqrt{\gamma R T_1}} \qquad (1)$$

$$\frac{T_5}{T_1} = \frac{\left\{2(\gamma-1)M_S^{\,2} + (3-\gamma)\right\}\left\{(3\gamma-1)M_S^{\,2} - 2(\gamma-1)\right\}}{(\gamma+1)^2 M_S^{\,2}} \qquad (2)$$

where a is the speed of sound in test gas mixture, γ is the specific heat ratio of test gas mixture, R is the gas constant and T_1 is the temperature of test gas mixture.
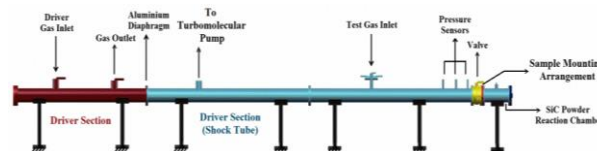

Fig. 1. Schematic diagram of the material shock tube (MST1) used for exposing SiC fine powders to shock treatment.

In the present set of experiments the SiC samples were exposed to shock wave with an estimated reflected shock temperature (T_5) and pressure (P_5) of about 4800 − 5300 K at P_5 of 22−25 bar for 1−2 ms duration. During shock exposure the sample experiences reflected shock temperature and pressure in the SiC reaction chamber, after shock experiment the solid residue left in the SiC reaction chamber was collected for further characterization using different experimental techniques. Similar procedures were repeated for the collected solid residues after each shock treatment.

Characterization

Various experimental techniques were used to characterize the SiC samples before and after shock treatment. Powder X-ray diffractometer (XRD) with Cu Kα (λ = 1.5418 Å) radiation is used to study the changes in crystal structure (PANalytical Empyrean). Scanning electron microscope (SEM) was used to study the surface morphology of SiC powders before and after shock impact (FEI Quanta 250 FEG). High resolution transmission electron microscopy (HRTEM)

was used to record bright field images, HRTEM images and selected area electron diffraction (SAED) along with the energy dispersive spectroscopy (EDS) for elemental analysis (FEI Tecnai F30 S-TWIN TEM). X-ray photoelectron spectroscopy (XPS) study was carried out using Al Kα (1486.6 eV) radiation to understand the chemical composition and electronic structure of SiC before and after shock treatment (AXIS Ultra DLD, Kratos Analytical). Low energy electron flood gun was used to nullify the charge accumulation on the surface of insulating sample. XPS spectra were recorded by mounting the powder samples on carbon tape. The position of C1s peak at binding energy 284.6 eV was taken as reference with an accuracy of ± 0.1 eV for calibrating the spectra if any shift in the binding energy.

Results and discussion

XRD patterns of SiC fine powder before and after exposure to shock-treated O_2 are shown in **Fig. 2**. Pristine SiC powder (before shock) shows hexagonal crystal structure with lattice parameters a = b = 3.08 Å and c = 15.12 Å and with prominent diffraction lines of hkl value (006) at 2θ = 35.6° (JCPDS No. 01-074-1302 and *SG* no.: P6$_3$mc) and other diffraction lines at (101), (103), (104), (107), (108), (109) and (116) corresponding to 2θ at 34°, 35.6°, 38.1°, 41.4°, 54.6°, 65.6° and 71.7° as shown in **Fig. 2**. After 1, 2 and 3 shock treatments the XRD patterns of the SiC shows reduced intensity of peak at 2θ = 35.6° as shown in **Fig. 2**. Sample shows mixed phase of SiC and SiO_2 in hexagonal and amorphous phases, respectively. After the 4 shock treatment, XRD pattern shows very less crystalline SiC and maximum SiO_2 in amorphous phase at 22° as shown in **Fig. 2** (4-shock).
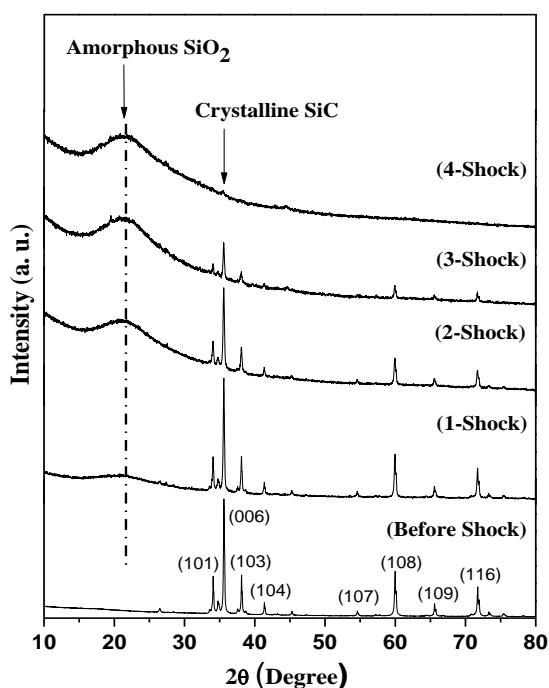
The changes in full width half maximum (FWHM) of respective XRD patterns are attributed to change in particle size and crystalline nature of SiC after multiple shock treatments. Increase in FWHM of the intense XRD peak at 2θ = 35.6° from 0.154° to 0.256° is a signature for the reduction in the average particle size of the samples from 154 nm to 53 nm which was calculated from scherrer's formula shown in equation (3):

$$D = \frac{k\lambda}{\beta_{calculated} \cos \theta} \qquad (3)$$

where D is the particle size, k is the instrument shape factor, λ is wavelength of X-ray, $\beta_{calculated}$ is the FWHM of peaks and θ is the diffraction angle. The decrease in average particle sizes are due to the various factors such as melting, re-crystallization and strain developed after shock interaction. **Fig. 3a** depicts the average particle size of SiC at each shock treatment and after 4-shock treatment SiC shows spherical particle of about 53 nm.

Intensity of the crystalline SiC and amorphous SiO_2 peaks indicate the percentage of crystallinity of SiC powder as shown in **Fig. 3b**. The degree of crystallinity (χ_c) of SiC was calculated using Hermans-Weidinger method as represented in equation (4):

$$\chi_c = \frac{A_{crystalline}}{A_{crystalline} + kA_{amorphous}} \qquad (4)$$

where χ_C is the degree of crystallinity, k is the instrument shape factor (0.9), $A_{crystalline}$ and $A_{amorphous}$ are the area under the curves of the crystalline and amorphous peaks of SiC and SiO_2, respectively. The area under the curves of the crystalline SiC and amorphous SiO_2 peaks are used to calculate the χ_c. The trend of change of crystalline SiC to amorphous SiO_2 on multiple shock treatment is shown in **Fig. 3b**.

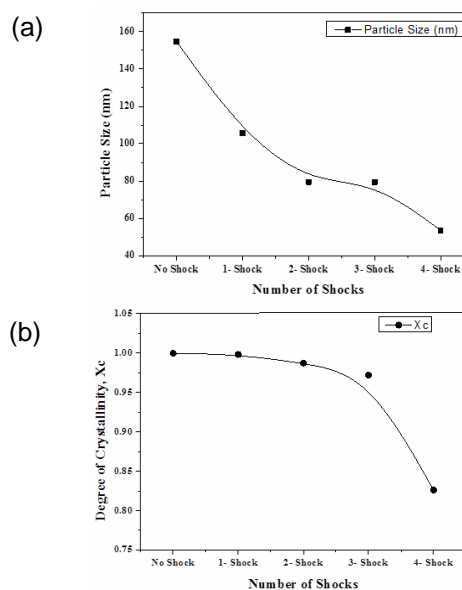**Fig. 2.** XRD patterns of SiC: before shock, after 1-shock, 2-shock, 3- shock and 4-shock treatment.

Fig. 3. (a) Variation of average particle size of SiC after each shock treatment, (b) Variation of Degree of crystallinity of SiC samples after each shock treatment.
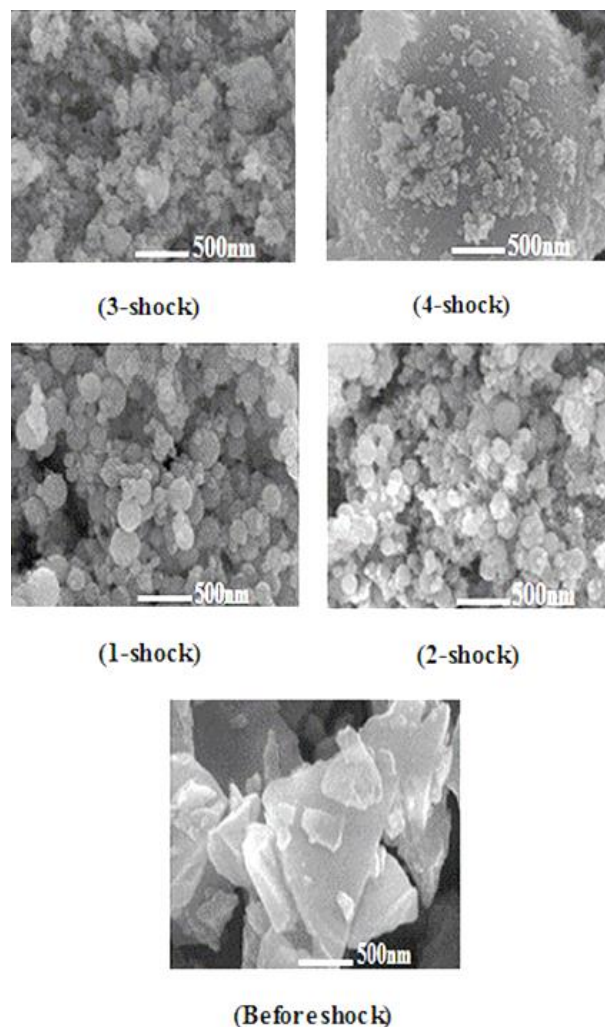
Fig. 4. SEM micrographs of SiC before and after each shock treatment.

SEM micrograph shows the surface morphology of the SiC fine powders before and after shock treatment as represented in **Fig. 4.** Figure 4 shows the irregular particles of SiC before shock treatment. The shock-treated samples show spheres of various sizes ranging from 45 nm to 10µm due to melting, nucleation and growth of particles during shock treatment in millisecond timescale.

TEM studies provide inferences about the change in morphology of the SiC particles from irregular to spherical shape after shock treatment. The bright field images confirm the change in morphology of the particles before and after each shock exposure as shown in **Fig. 5a**. HRTEM micrographs of crystaline SiC before shock treatment show diffraction fringes with lattice spacing of about 0.232 nm, after shock treatment the diffraction fringes are not visible due to amorphous nature of SiO_2 as shown in **Fig. 5b**. SAED pattern of crystalline SiC shows the ordered bright electron diffraction pattern indexed at 103, 105, 109 and 201 corresponding to the pristine SiC sample, but after each shock treatment it shows diffused rings due to amorphous nature as shown in **Fig. 5c**.
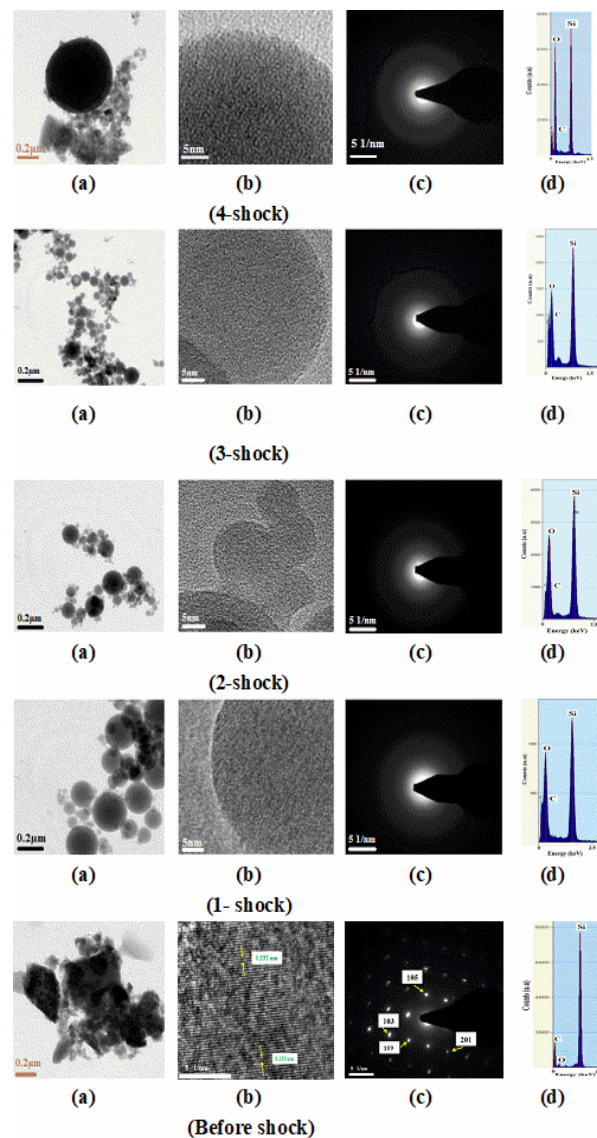

Fig. 5. TEM micrographs of SiC before and after each shock treatment.

The formation of SiO_2 in amorphous phase has been confirmed by EDS analysis which reveals the atomic percentage of different elements present in the samples before and after impact of shock-heated oxygen gas. Before shock treatment the sample contains a negligible amount of oxygen (~2%) but after each shock exposure the EDS shows increasing oxygen percentage in the samples due to oxidation as represented in **Fig. 5d**. According to Figure 5d, after four shock treatment the carbon content is reduces to about 24% which gives rise to increasing oxygen content by 50% that confirms the formation of amorphous SiO_2 due to oxidation of SiC.

XPS study has been performed on SiC fine powders before and after exposure to shock heated oxygen gas to analyze its chemical, electronic state and elemental composition. XPS of Si2p core levels shows binding energy peaks at 99.5, 100.2, 101.3 and 103.1 eV due to the presence of Si–Si, Si–C, Si–O–C
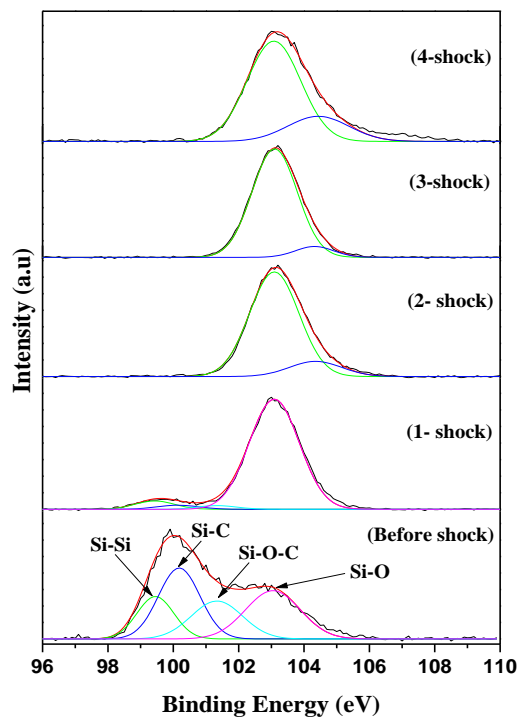
Fig. 6. XPS of Si2p core levels of SiC before and after each shock treatment.

and Si−O species, respectively as shown in **Fig. 6**. The carbide and oxycarbide peaks after 1-shock exposure decreases in intensity in comparison with that of pristine sample as presented in **Fig. 6**. After subsequent shock treatments (2, 3 and 4-shocks) oxycarbide and other associated carbide species are completely oxidized to form silicon dioxide which can be understood from the spectra shown in **Fig. 6**. Si2p core level peaks at 100 and 103 eV due to Si−C and Si−O, respectively have been reported in the literature [8, 26]. The formation of Si−OH bond at 104.3 eV after 4-shock treatment, may be due to the presence of hydrocarbon as shown in **Fig. 6**. Deconvoluted C1s XPS spectra show a peak at 282.1 eV due to C−Si and other peak at 284.6 eV from graphitic carbon, which is used to calibrate the shift in binding energies in XP spectra. The peaks at 286 and 288.5 eV represent C−O and C=O bond due to the presence of carbide/oxy-carbide species as shown in **Fig. 7a**. After each shock exposure C1s peak due to C−Si reduces in intensity and finally vanishes after 4-shock retaining the oxycarbide peak as shown in **Fig. 7a.**

Reduction in C−Si peak after 4-shocks at 282.1 eV is a clear indication of oxidation of SiC occured after shock treatment as shown in **Fig. 7a**. O1s spectra show the native O−O peak at 532.1 eV and a peak at 533.2 eV due to presence of small SiO₂ species before shock as shown in **Fig. 7b**. After each shock exposure (1, 2, 3, and 4-shock) the ratio of intensity of O−O peak to Si−O peak reduces from ~3 to ~0.5. Conversely, there is a significant increase in the intensity of Si−O peak in the subsequent shocks shows increase in oxygen concentration.
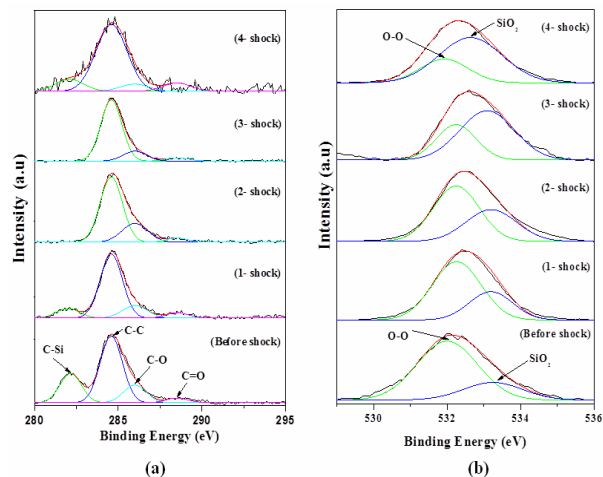

Fig. 7. (a) XPS of C1s core levels of SiC before and after each shock treatment, (b) XPS of O1s core levels of SiC before and after each shock treatment.

XPS of O1s core levels confirms that SiC has converted to SiO₂ after multiple shock treatments in presence of oxygen test gas as shown in **Fig. 7b**. XPS confirms the presence of SiO₂ after multiple exposures of SiC to shock heated oxygen test gas within 4 shocks which amounts to total exposure time of SiC for about 5–10 ms.

SiC undergoes non-catalytic surface reaction in presence of shock-heated oxygen test gas for short duration due to super heating and cooling. During the process, metastable compounds like sub-oxycarbides $SiOC_3$, SiO_2C_2, SiO_3C and sub-oxides like SiO_2, SiO and Si_2O_3 are formed after multiple shock exposures. The schematic diagram of the reaction mechanisms is shown in **Fig. 8**. The possible reactions occurred by forming final stable product like SiO₂ in solid phase and SiO in gas phase are listed below in Eqs. (5) and (6):
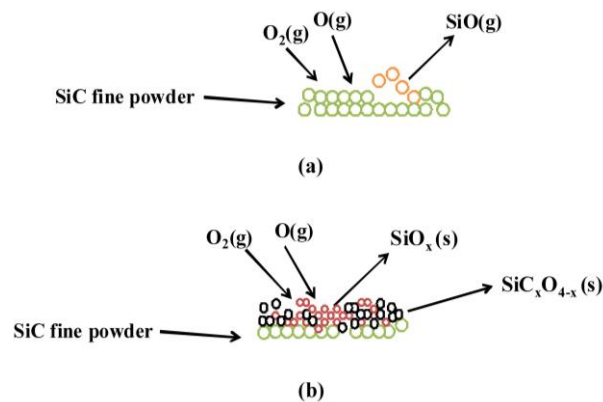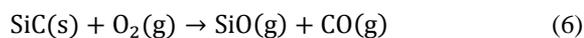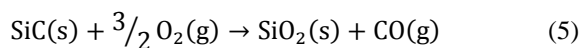
$$SiC(s) + \frac{3}{2}O_2(g) \rightarrow SiO_2(s) + CO(g) \tag{5}$$

$$SiC(s) + O_2(g) \rightarrow SiO(g) + CO(g) \tag{6}$$

Fig. 8. Schematic diagram of the SiC powder interaction with strong shock heated oxygen.

Conclusion

SiC fine powders have been treated in presence of shock-heated ultra high pure Ar+O$_2$ gas mixture using MST1 to study its phase transformation and oxidation resistance at different dynamic shock strengths. UHP oxygen has been exposed to shock wave (estimated reflected shock temperature of 4800−5300 K and 22−25 bar pressure) for short duration to interact with the pure SiC fine powder. The change in crystal structure from hexagonal SiC to amorphous SiO$_2$ is evident from the XRD and TEM studies. The degree of crystallinity of SiC decreases upon multiple shock treatments. SEM and TEM micrographs of pristine SiC show irregular particles and after every shock impact the particles are found to be in spherical shape of different sizes. The Si2p core level spectra show the formation of SiO$_2$ and SiO$_x$C$_y$ due to the oxidation of SiC, further on subsequent shock exposures SiO$_x$C$_y$ completely oxidizes and forms amorphous SiO$_2$. SiC undergoes three-body non-catalytic surface reactions respectively between the shock-heated oxygen gas and the SiC powder. Such reactions are similar to the one which occur on the surface of space vehicles during atmospheric re-entry. This novel dynamic shock exposure technique is developed in our laboratory and used to study oxidation properties of SiC fine powders for the first time in millisecond timescale which is distinct from the conventional shock produced by flyer/projectile impact. Even though the study of oxidation of SiC has been done by several techniques, in the present study oxidation of SiC is done in a small duration under extreme aero-thermodynamic condition which is not reported in the literature. Also the oxidation studies of SiC using conventional furnace are done for a longer duration and the thermodynamic conditions generated by shock tubes are difficult to reproduce by furnaces. Further, to understand the chemistry of materials in millisecond timescale for a given experimental condition needs thorough thoretical and molecular dynamic (MD) simulation studies.

References

1. Badini, C.; Liedtke, V.; Euchberger, G.; Celasco, E.; Biamino, S.; Marchisio, S.; Pavese, M.; Fino, P.; *J. Eur. Ceram. Soc.*, **2012**, 32, 4435-4445.
   DOI: 10.1016/j.jeurceramsoc.2012.07.031
2. Fahrenholtz, W. G.; and Hilmas, G. E.; *Intl. Mater. Rev.*, **2012,** 57, 61.
   DOI: 10.1179/1743280411Y.0000000012
3. Amico, G. C. D'.; Ortona, A.; Biamino, S.; Fino, P.; Badini, C.; Angelo, C. D'.; *Adv Engn Mater.*, **2016**, 16(2), 176.
   DOI: 10.1002/adem.201300261
4. Ben-aim, R. I.; Bonardet, J. L.; Diamy, A. M.; Fraissard. J.; Legrand, J. C.; *J. Mater. Sci.*, **1990**, 25, 4113-4119.
   DOI: 10.1007/BF00582490
5. Roy, J.; Chandra, S.; Das, S.; Maitra, S.; *Rev. Adv. Mater. Sci.*, **2014** 38, 29-39.
   ISSN: 16065131
6. Gianella, S.; Gaia, D.; Ortona, A.; *Adv. Engn. Mater.*, **2012**, 14, 1074−1081.
   DOI: 10.1002/adem.201200012
7. Wright, N. G.; Horsfall, A. B.; *J. Phys. D: Appl. Phys.*, **2007** 40, 6345-6354.
   DOI: JPhysD/40/6345
8. Önneby, C.; Pantano, C. G.; *J. Vac. Sci. Technol*. A., **1997**, 15(3), 1597-1602.
   DOI: 10.1116/1.580951
9. Wagner, C.; J. Appl. Phy., **1958**, 29(9), 1295-1297.
   DOI: 10.1063/1.1723429
10. Han, J.; Hu, P.; Zhang, X.; Meng, S.; Han, W.; *Comp. Sci. Tech.*, **2008**, 68(3-4), 799-806.
    DOI: j.compscitech.2007.08.017
11. Williams, P. A.; Sakidja, R.; Perepezko, J. H.; Ritt, P.; J. Eur. Ceram. Soc., **2012**, 32, 3875-3883.
    DOI: j.jeurceramsoc.2012.05.021
12. Lamouroux, F.; and Camus, G.; *J. Eur. Ceram. Soc.*, **1994**, 14(2), 177-188.
    DOI: 10.1016/0955-2219(94)90105-8
13. Li, T.; Duan, Y.; Jin, K.; Suo, T.; Yu, X.; Li, Y.; *Int. J. Imp. Engnn.*, **2017**, 109, 391-399.
    DOI: 10.1016/j.ijimpeng.2017.08.001
14. Gu, Y. B.; Ravichandran, G.; *Int. J. Imp. Engnn.*, **2006**, 32, 1768-1785.
    DOI: 0.1016/j.ijimpeng.2005.04.012
15. Lespade, P.; Richet, N.; Goursat, P.; *Acta. Astrn.*, **2007**, 60, 858-864.
    DOI: 10.1016/j.actaastro.2006.11.007
16. Pourasad, J.; Ehsani, N.; Khalifesoltani, S. A.; *J. Eur. Ceram. Soc.*, **2016**, 36, 3947-3956.
    DOI: 10.1016/j.jeurceramsoc.2016.06.046
17. Poorteman, M.; Descamps, P.; Cambier, F.; Plisnier, M.; Canonne, V.; Descamps, J. C.; *J. Eur. Ceram. Soc.*, **2003**, 23, 2361-2366.
    DOI: 10.1016/S0955-2219(03)00088-8
18. Monteverde, F.; and Scatteia, L.; *J. Am. Ceram. Soc.*, **2007**, 90(4), 1130-1138.
    DOI: 10.1111/j.1551-2916.2007.01589.x
19. Kondo, K. I.; Soga, S.; Sawaoka, A.; Araki, M.; *J. Mater. Sci.*, **1985**, 20(3), 1033-1048.
    DOI: 10.1007/BF00585748
20. Kurdyumov, A. V.; Britun, V. F.; Yarosh, V. V.; Danilenko, A. I.; *Pow. Metall. Met. Ceram.*, **2015**, 54(7-8), 381-389.
    DOI: 10.1007/s11106-015-9726-3
21. Orphal, D. L.; and Franzen, R. R.; *Int. J. Imp. Engnn.*, **1997**, 19(1), 1-13.
    DOI: 10.1016/S0734-743X(96)00004-8
22. Thanganayaki, N.; Reddy, K. P. J.; Jayaram, V.; Oxidation resistance studies of silicon carbide thin film in a free piston-driven shock tube, ISSW29, 14-19 July, Madison, Wisconsin, U.S.A., *1*, 1431-1436, **2013**.
23. Ravindra, N. G.; Chen, W.; Tong, F, M,; Nanda, A. K.; Speranza, A. C.; *IEEE Trans. Semicond. Manuf.*, **1998**, 11(1), 30-37.
24. Jayaram, V.; and Reddy, K. P. J.; *Adv. Mater. Lett.*, **2016**, 7(11), 100-150).
    DOI: 10.5185/amlett.2016.6379
25. Gaydon, A. G.; Hurle, I. R.; The Shock Tube in High - Temperature Chemical Physics; Reihold Publishing Corporation: New York, **1963**.
26. Sreemany, M.; Ghosh, T. B.; Pai, B. C.; Chakraborty, M.; *Mat. Res. Bull.*, **1998**, 33(2), 189-198.
    DOI: 10.1016/S0025-5408(97)00222-5